Biosensors and Bioelectronics 162 (2020) 112253

Contents lists available at ScienceDirect

Biosensors and Bioelectronics

journal homepage: http://www.elsevier.com/locate/bios

Integrated individually electrochemical array for simultaneously detecting multiple Alzheimer's biomarkers

Yongchao Song [a], Tailin Xu [a,*], Qinglin Zhu [a], Xueji Zhang [b,**]

[a] Research Center for Bioengineering and Sensing Technology, University of Science and Technology Beijing, Beijing, 100083, PR China
[b] School of Biomedical Engineering, Shenzhen University Health Science Center, Shenzhen, Guangdong, 518060, PR China

ARTICLE INFO

Keywords:
Mini-pillar array
Gold nanodendrites
Multiple biomarkers
Simultaneous detection

ABSTRACT

Simultaneous detection of multiple biomarkers is benefit for reducing the detection cycles, avoiding the false-positive signals, and providing the cross validation, which provide the opportunity to understand the pathogenic mechanisms and achieve precise early diagnosis. Here, we demonstrate the mini-pillar-based individual electrochemical array for simultaneous detection of multiple biomarkers. On such platform, the mini-pillar could confine the microdroplet as individual and open-channel microreactor, which is extremely helpful for reducing reagent consumption and extracting internal information, and the electrodes array embedded in mini-pillar are integrated on one side to achieve multiple and simultaneous electrochemical sensing. The introduction of gold nanodendrites by electrodeposition has greatly enhanced sensitivity via improving probe-binding capacity and response signals. Sensitive and selective detection of multiple Alzheimer's biomarkers including Tau, ApoE4, Amyloid-β and miRNA-101 on such mini-pillar-based biosensor is also achieved. Such biosensor platform with the advantages of high-yield, high sensitivity, low-waste and multiple signals output shows great promise in sensing multiple biomolecules for disease diagnosis and health monitoring.

1. Introduction

The biomarkers including proteins, nucleic acids and metabolites are designated as indicators that can be objectively measured and evaluated for a normal biological process, pathogenic process, or pharmacological responses to a therapeutic intervention(Chan et al., 2017; Chi, 2016; Kalinich and Haber, 2018; Perfezou et al., 2012; Ye et al., 2018a). Recently, tremendous efforts have focused on sensing correlative biomarkers by various promising technologies including electrochemical, colorimetric methods, fluorescence assay and surface enhanced Raman spectroscopy (SERS) for understanding the pathogenic mechanisms and achieving diseases early diagnosis(Brodbelt et al., 2019; Ding et al., 2016; Hwang and Myong, 2014; Labib et al., 2016; Li et al. 2015a, 2015b, 2019; Song et al., 2011). However, most diseases are accompanied by abnormal regulation of multiple biomarkers that no single biomarker can accurately predict(Ho et al., 2016; Perrin et al., 2009; Safikhani et al., 2017; Savelieff et al., 2018; Xu et al., 2017a; Zhao et al., 2015). Thus, the sensing platforms tend to integration, parallelization and multiplexing for simultaneous and multiple analysis of numerous components toward precise disease early diagnosis.

The open-channel systems that manipulate and functionalize the droplets in well-defined areas have been advanced in both fundamental investigations and technological applications such as biology, synthetic industry, and biosensors(Atobe et al., 2018; Feng et al., 2018; Kutter et al., 1998; Li et al., 2016; Popova et al., 2018; Xu et al., 2019). As main open-channel platform, superwettable wells and mini-pillar surface without skilled technicians and sophisticated instrumentation, have presented the compartment, monodispersity and low-volumes for diversified applications such as photonics and near-field imaging, nanomaterial synthesis, digital polymerase chain reaction, and cell analysis(Faltova et al., 2018; Huebner et al., 2008; Lee et al., 2018; Su et al., 2018; Xu et al., 2017b; Zhu et al., 2018). Importantly, openness microreactors are accessible to match with automation equipment for dealing with large numbers of samples and substantially couple with electrochemical, SERS, colorimetric, and fluorescence devices for sensitively and selectively sensing(He et al. 2018, 2019; Hou et al., 2014; Shin et al., 2017; Song et al., 2019; Xu et al., 2015). Thus, much efforts have focused on employing the open-channel microreactors to achieve high-throughput and multiple analysis.

Herein, we demonstrate the mini-pillar-based individual

* Corresponding author.
** Corresponding author. School of Biomedical Engineering, Shenzhen University Health Science Center, Shenzhen, Guangdong, 518060, PR China.
E-mail address: xutailin@ustb.edu.cn (T. Xu).

https://doi.org/10.1016/j.bios.2020.112253
Received 12 February 2020; Received in revised form 24 April 2020; Accepted 26 April 2020
Available online 5 May 2020

electrochemical array that confines the reagent in open-channel microreactors for simultaneously sensing multiple biomarkers. On such electrochemical sensor, the mini-pillar can entrap the trace analytes to form open-channel microreactor, and the electrodes array can extract the electrochemical signals to complete high-throughput and simultaneous sensing. The gold nanodendrites is obtained by electrodeposition onto the working electrode, and its optimal morphology with optimal electrochemical performance is obtained by regulating deposition parameters including potential, time and electrolyte concentration. Such mini-pillar-based sensor with the advantage of enabling more biomarkers detection simultaneously and sensitively compared to traditional methods (SI Table 1) has detected the multiple Alzheimer's biomarkers including Tau, ApoE 4, Amyloid-β and miRNA-101, showing great potential for the disease early diagnosis and health monitoring.

2. Materials and experiments

2.1. Materials and reagents

Ethanol (>99.8%, GR), acetone, hexaammineruthenium (III) chloride, bovine serum albumin and phosphate buffer saline (PBS) were purchased from Sigma-Aldrich. Hydrogen tetrachloroaurate (III) trihydrate ($HAuCl_4 \bullet 3H_2O$) and sodium chloride were purchased from Alfa Aesar. The PDMS was purchased from Dow Europe GmbH. The template with array was custom made from Beijing Zhongjingkeyi Technology Co., Ltd, China. The Tau, ApoE 4 and Amyloid-β antigen were purchased from Pepro Tech. The Tau, ApoE 4 and Amyloid-β antibodies were purchased from Abbkine. All chemicals were used without any further purification and prepared by dilution using ultrapure water (Milli-Q, 18.2 MΩ cm) otherwise specified.

The target DNA and miRNA-101 were obtained by SangonBiotech (Shanghai, China). The sequences were as follows:

MiRNA-101: 5′-UAC AGU ACU GUG AUA ACU GAA G-3′

Target DNA: 5′-Fc-(CH_2)6-TTAGCCTTCAGTTATCACAGTACTGTA-GCTAA-(CH_2)6 -SH-3′

2.2. Fabrication of PDMS mini-pillar sensor

The single-sided printed integrated circuit board was customized from the manufacturer. The PDMS prepolyme and curing agent were mixed with the ratio of 15:1 and bubbles were cleared by the vacuum drying oven. Then the prepolymer was poured on the prepared polytetrafluoroethylene (PTEE) template (Fig. S1b) with the through-holes in 80 °C and flew into holes of template forming the mini-pillar of ~5 mm in diameter and of ~1.65 mm in height. Next, the electrodes array (Au as working electrode, Pt as counter electrode, and Ag as reference electrode) were embedded in incomplete solidification mini-pillars. After stripped the mini-pillar platform, the mini-pillar platform with electrode array was glued on the flexible integrated circuit board by the adhesive of prepolymer and cyclohexane (ratio of 1:1), and we obtained the mini-pillar sensor.

2.3. Fabrication of nanodendrites gold on mini-pillar sensor

The array of mini-pillars was respectively dropped 10 μL electrolyte with specified $HAuCl_4$ concentration, and the interdigital electrode fingers of integrated circuit board were connected with electrochemical workstation. After set the deposition parameters (potential and time), we began to fabricate the nanodendrites gold on working electrodes. The nanodendrites gold with different surface area were simultaneously obtained on mini-pillar sensor for further electrochemical performance study and biomarkers sensing.

2.4. Electrochemical performance investigation of different nanodendrites gold

The nanodendrites gold on working electrodes was firstly cleared by ethanol, acetone and ultrapure water. The 10 μL 10 mM PBS (pH 7.4) containing 5 mM $Ru(NH_3)_6^{3+}$ and 0.1 M NaCl were dropped on mini-pillar for square wave voltammetry (SWV) measurement from −0.5 to −0.1 V with a step potential of 5 mV, a frequency of 15 Hz, and an amplitude of 50 mV. After the electrochemical signals comparison, we chose the optimized nanodendrites gold for further electrochemical biomarkers sensing.

2.5. Electrochemical detection of proteinaceous biomarkers on mini-pillar sensor

The detection possesses of proteinaceous biomarkers including Tau, ApoE 4, Amyloid-β were consistent. The 10 μL droplet with 10^{-6} mg/mL antibody was dropped on mini-pillar, and incubated at room temperature for 4 h for antibody adsorption on the nanodendritic gold surface. Then the 10 μL 1 mg/mL BSA were used to block the nanodendritic gold surface for avoiding non-specific adsorption during detection. The excess antibody and BSA that was not adsorbed was removed by ultrapure water. The 10 μL 10 mM PBS (pH 7.4) containing 5 mM $Ru(NH_3)_6^{3+}$ and 0.1 M NaCl were dropped on mini-pillar for recording the electrochemical signals by square wave voltammetry from −0.65 to 0.05 V. Then 10 μL antigen concentration of 10^{-10}, 10^{-9}, 10^{-8}, 10^{-7} mg/mL were dropped on mini-pillar for 4 h at room temperature for antibody's specific recognition. Rinsed out excess antigen and recorded the latest electrochemical signals consistent in 10 μL 10 mM PBS (pH 7.4) containing 5 mM $Ru(NH_3)_6^{3+}$ and 0.1 M NaCl by square wave voltammetry from −0.65 to 0.05 V. Then compared electrochemical signals change and recorded the signal fluctuations (ΔI). Signal fluctuations are used to assess the concentration of the target biomarkers.

2.6. Electrochemical detection of miRNA-101 on mini-pillar sensor

The 10 μL 10^{-6} M probe DNA was dropped on mini-pillar, and the probe DNA immobilized and automatically ring on the nanodendritic gold surface at room temperature for 4 h. Rinsed out unfixed probe DNA and recorded the electrochemical signals in the looped state in 10 mM PBS (pH 7.4) containing 5 mM and 0.1 M NaCl by square wave voltammetry (SWV) from −0.05-0.15 V. Then target miRNA-101 (10 μL) with concentration of 10^{-10}, 10^{-9}, 10^{-8}, 10^{-7} M was incubated on mini-pillar for 4 h. Then record the latest electrochemical signals of the probe DNA conformational change in 10 mM PBS (pH 7.4) containing 5 mM and 0.1 M NaCl by square wave voltammetry (SWV) from −0.05-0.15 V. Then compared electrochemical signals change and recorded the signal fluctuations (ΔI). Signal fluctuations were used to assess the concentration of the target biomarkers.

3. Results and discussion

3.1. Choice of materials

The mini-pillar-based electrochemical sensor mainly consists of microdroplets manipulation unit and electrochemical transmission unit. The PDMS with the preponderances of simple preparation, good biocompatibility, nontoxicity, hydrophobicity and flexibility is employed to the mini-pillar platform for microdroplets manipulation. The individual three-electrode in mini-pillar (Au as working electrode; Pt as counter electrode; Ag as reference electrode) is the most common electrochemical system for signals transmission. While the bare gold working electrode is different to meet the high sensitivity sensing in microdroplet. Thus, we employ the electrodeposited method for the modification of working electrode and choose the gold nanomaterials for improving the sensitivity and immobilizing probe DNA by Au–S

bond. The optimized gold nanodendrites electrodes is achieved by investigating the multiple deposition parameters for subsequent multiple biomarkers sensing.

3.2. Characterization of the mini-pillar-based electrochemical sensor

The mini-pillar-based electrochemical sensor shows the unique ability of forming the individual and parallelizable open-channel microreactors for multiple and simultaneous sensing biomarkers. As schematically demonstrated in Fig. 1, such biosensor mainly consists of mini-pillar unit with electrodes array and the circuit integration unit. The PDMS mini-pillar has high adhesion performance for anchoring the droplets, and the embedded electrode array where the Au as working electrode, Pt as counter electrode, and Ag as reference electrode collect the electrochemical signals in open-channel reactors. With the assistance of gold nanodendrites that deposited on working electrode, such mini-pillar-based sensor has greatly improved the probe-binding capacity and the response signals for sensitively electrochemical sensing. The circuit integration unit is the single-sided printed on circuit board as shown in Fig. S1a, the end face of the interdigital electrode fingers is designed to connect a multi-channel electrochemical workstation for monitoring multiple signals.

3.3. Optimization of the gold nanodendrites electrodes

The gold nanodendrites on working electrode is of great significance for enhancing the unprecedented sensitivity, which profoundly affects both thermodynamics and kinetics of the assembly, binding and signal transduction of biomarkers (Das et al., 2012; Ye et al., 2018b). We investigated multiple deposition parameters including the potential, time and electrolyte concentration as shown in Fig. 2. Firstly, the potential influence was explored at the voltages ranging from −0.1 V to −1.0 V (10 μL 10 mg/mL $HAuCl_4$ for 1000s). Large quantities of irregular gold nanoparticles were dispersed on working electrode at low potential (−0.1 V) with a feeble electrochemical signal (Fig. 2a). As the potential shifted to −0.3 V, partial gold nanoparticles were staggered to form hierarchical morphology with persistent weak electrochemical signal as shown in Fig. 2b. Subsequently, the representative spherical gold nanoparticles were observed at −0.5 V with the enhancement of electrochemical signal (Fig. 2c). As shown in Fig. 2d, the gold nanodendrites emerged with the potential rising to −0.8 V, and the finely nanotextured arms and branches provided the extensive active surface area for electronic transmission with tremendous electrochemical signal. When applied the −1.0 V, the morphology was still the dendritic-type while more gold nanoparticles decorated in gap of nanotextured arms and branches causing the shrinking electrochemical signals (Fig. 2e).

Then, we evaluated the influence of deposition time from 100 s to 1000 s on gold morphology and electrochemical performance in 10 μL 10 mg/mL $HAuCl_4$ at −0.8 V. The gold nanoparticles had an initial reduction and gradually prone to agglomerate and complicated with weak electrochemical response in 100 s (Fig. 2f). When the time prolonged to 300 s, the irregular morphology translated to the nanodendritic-type with an innovative signal (Fig. 2g). With the time extension from 500 to 800 s (Fig. 2h and i), the gold nanodendrites possessed higher density and active surface area with increasing electrochemical signal. However, the morphology of gold nanodendrites in 1000 s had an ignorable decrease, which may cause by partial gold nanodendrites shedding (Fig. 2j). The electrolyte influence was investigated at the $HAuCl_4$ concentration ranging from 0.1 to 1.0 mg/mL (−0.8 V in 10 μL $HAuCl_4$ for 800 s). In low concentration, the rare gold ions were not enough to from nanodendrites (1 mg/mL, Fig. 2k) with feeble electrochemical signal. When the concentration was increased to 3 mg/mL, the electrochemical signal was significantly enhanced as shown in Figure 2l. With the concentration increasing from 5 to 10 mg/mL (Fig. 2m–o), the nano-gold morphology maintained the uniform nanodendritic-type and consistent electrochemical performance. Thus, we employed the 10 μL 5 mg/mL $HAuCl_4$ at −0.8 V for 800 s as the optimal conditions for fabrication of gold nanodendrites.

3.4. Electrochemical performances of the mini-pillar sensor

The electrochemical performances of the mini-pillar sensor with modification of gold nanodendrites were systematically characterized as shown in Fig. S2. Cyclic voltammograms (Scan rate: 100 mV/s) carried out in 10 mM PBS (pH 7.4) containing 5 mM $Ru(NH_3)_6^{3+}$ and 0.1 M NaCl before and after reduction of gold nanodendrites as shown in Fig. S2a. The current response of gold nanodendrites electrode (red trace) toward $Ru(NH_3)_6^{3+}$ was larger than that of bare Au, suggesting that the electrochemical active sites of working electrode increased by gold nanodendrites. In order to understand the charge transport characteristics of the gold nanodendrites electrode, we recorded cyclic voltammograms at various scan rates from 10 to 250 mV/s between −0.5 and + 0.1 V as shown in Fig. S2b. The anodic and cathodic peak currents increased and peak potential remained almost unchanged with the increase of scan rates, indicating the redox process on gold nanodendrites electrode is a surface-confined process. Moreover, the gold nanodendrites fabricated in optimal deposition conditions were extremely stability with the ignorable electrochemical signal fluctuation resisting washing of 30, 60, 90, 120 and 150 s as shown in Fig. S2c. Thus, the nanodendrites gold-assisted mini-pillar biosensor with high sensitivity and stability is suitable for electrochemical detection of multiple trace markers.

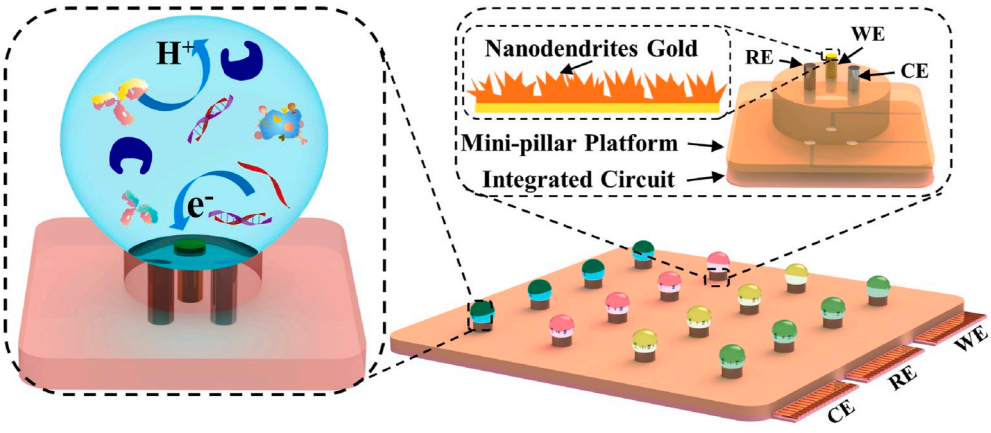

Fig. 1. Illustration of open-channel mini-pillar sensor for multiple electrochemical detection.

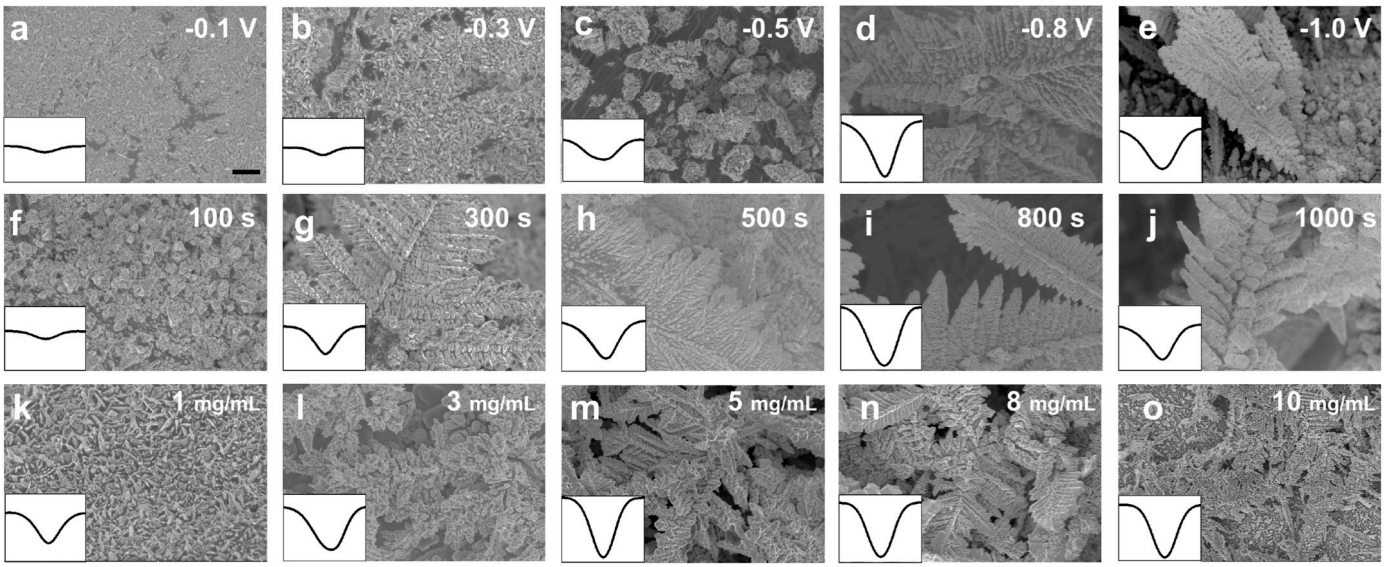

Fig. 2. Effect of the different deposition parameters on the gold nanostructures and electrochemical performance. The gold nanostructure at different deposition potential: a) −1.0, b) −0.3, c) −0.5, d) −0.8 and e) −1.0 V in 10 mg/mL $HAuCl_4$ for 1000 s and corresponding electrochemical signals. The SEM images and electrochemical responses of gold nanostructures at different deposition time: f) 100, g) 300, h) 500, i) 800 and j) 1000 s at −0.8 V in 10 mg/mL $HAuCl_4$. Different nanostructures and electrochemical performance of gold nanostructures at different $HAuCl_4$ concentration: h) 1, i) 3, j) 5, k) 8 and l) 10 mg/mL at −0.8 V for 800 s. All the electrochemical measurements carry out in 10 mM PBS containing 5 mM $Ru(NH_3)_6^{3+}$ and 0.1 M NaCl for square wave voltammetry.

3.6. *Electrochemical detection of the multiple Alzheimer's biomarkers*

Alzheimer's disease (AD) is broadly characterized by the deterioration of memory and cognition as the most common cause of dementia in the elderly (Chouraki and Seshadri, 2014; Roy et al., 2016; Zafari et al., 2015). The early diagnosis and intervention commences in preclinical and mild cognitive impairment stages represents an important strategy to restrict the prevalence of dementia. To evaluate the feasibility and versatility of such mini-pillar-based sensor, we performe simultaneous electrochemical detection of multiple Alzheimer's biomarkers. The mini-pillar-based individual electrochemical array shows potential to achieve high sensitivity detection of multiple Alzheimer's biomarkers

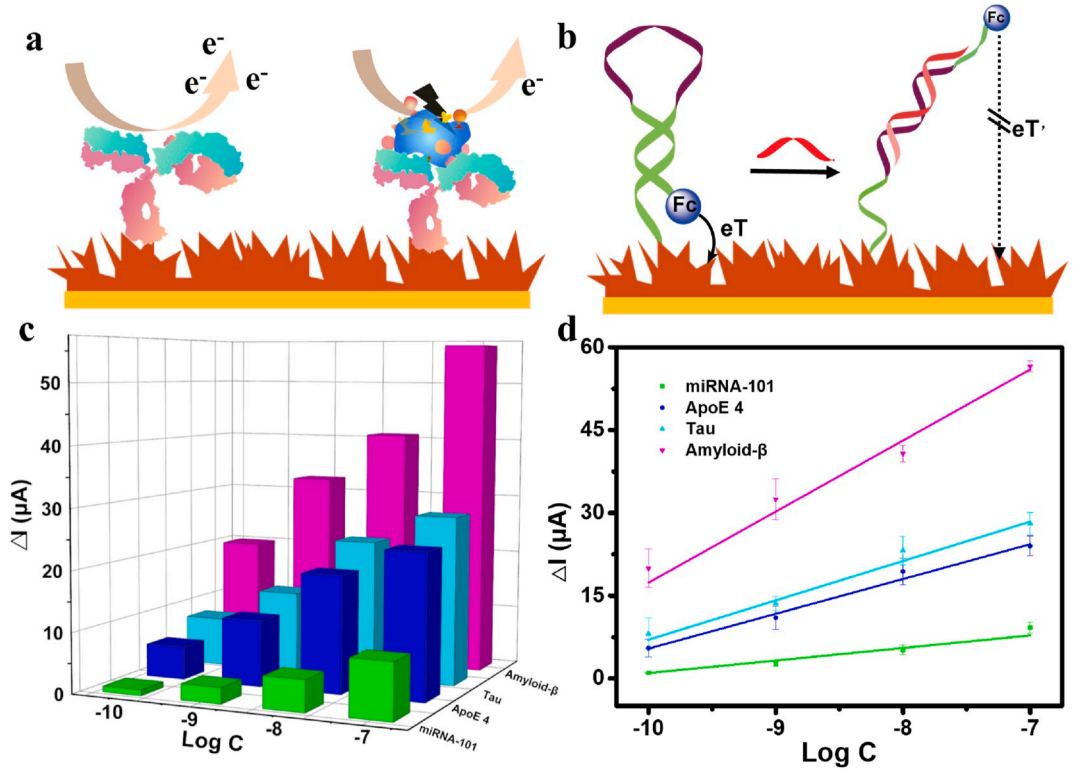

Fig. 3. Individual electrochemical array toward multiple and simultaneous sensing Alzheimer's biomarkers. a) The mechanism of electrochemical detection of proteinaceous biomarkers including ApoE4, Tau and Amyloid-β. b) The mechanism of electrochemical detection of miRNA-101. c) Electrochemical response of different concentration biomarkers (Green: miRNA-101; Blue: ApoE4; Cyan: Tau; Magenta: Amyloid-β) and the corresponding calibration curve (d). (For interpretation of the references to color in this figure legend, the reader is referred to the Web version of this article.)

including Tau, ApoE 4, Amyloid-β and miRNA-101. The detection of proteinaceous biomarkers including Tau, ApoE 4 and Amyloid-β is based on electrode resistance change with the electrochemical signals fluctuations as illustrated in Fig. 3a. We record the initial signal with the immobilizing of antibody and block protein on gold nanodendrites working electrode. When the antibody specifically recognizes the corresponding antigen, the surface resistance becomes large causing signal to decrease. The mechanism of miRNA-101 sensing is illustrated in Fig. 3b. The redox-reporter-modified hairpin DNA probe is immobilized on working electrode by Au–S bond with the large electrochemical signals. With the combining of miRNA-101, the conformational change alters the positioning of the reporter (Fc) relative to the electrode surface, thereby producing a target-dependent change in current. The signal fluctuations (ΔI) are used to assess the concentration of all the target biomarkers.

The electrochemical signals of multiple Alzheimer's biomarkers with different concentration have simultaneously recorded by mini-pillar-based sensor. As shown in Fig. 3c, **d**, current fluctuations (ΔI) of miRNA-101 are about 0.98 ± 0.02, 2.65 ± 0.21, 5.20 ± 0.88 and 9.20 ± 0.49 μA (n = 3) from 10^{-10} to 10^{-7} M, which show a good linear relationship with a correlation coefficient of 0.9605, and the detection limit is estimated to be 91.4 pM (S/N = 3). Similarly, current fluctuations (ΔI) of Tau are 8.1 ± 1.43, 13.58 ± 0.65, 23.2 ± 1.28 and 28.1 ± 0.99 μA (n = 3) from 10^{-10} to 10^{-7} mg/mL with the detection limit of 5.91×10^{-11} mg/mL (S/N = 3) and current fluctuations (ΔI) of ApoE4 from 10^{-10} to 10^{-7} mg/mL are 5.1 ± 0.81, 11 ± 1.04, 19.4 ± 1.21 and 24 ± 0.89 μA (n = 3) with the detection limit of 7.14×10^{-11} mg/mL (S/N = 3). For the Amyloid-β, the self-aggregation of antigen causes the large ΔI about 19.96 ± 1.73, 32.47 ± 1.84, 40.75 ± 0.75 and 56.56 ± 0.49 μA (n = 3) compared to Tau and ApoE 4, and a linear plot of ΔI ranging from 10^{-10} to 10^{-7} mg/mL is established with the detection limit of 8.6×10^{-12} mg/mL (S/N = 3). Subsequently, we investigate the selectivity of such mini-pillar sensor for multiple biomarkers sensing as shown in Fig. S3. The mini-pillar sensor can only respond to miRNA-101 when immobilized the specific probe DNA of miRNA-101. Similarly, antibody-modified mini-pillar sensors can only recognize the corresponding antigen regardless of interferential targets. Then, we detect the four multiple biomarkers in human serum sample on the mini-pillar sensor and compare the electrochemical results in PBS and serum as shown in SI Fig. 4. The electrochemical signal has negligible change in both systems, revealing the great potential for early diagnosis of Alzheimer's disease. Such mini-pillar sensor demonstrates the high sensitivity and selectivity for sensing multiple Alzheimer's biomarkers, while the nanodendritic gold material is costly compared to most biomarkers sensors and it is difficult to complete the detection of multiple biomarkers simultaneously in a single microdroplet. Thus, there is still much room to improve the mini-pillar sensor to meet high-demand clinical sensing.

4. Conclusions

In conclusion, the mini-pillar-based individual electrochemical array represents high sensitivity and selectivity for simultaneously sensing multiple biomarkers on one microchip. Such mini-pillar sensor mainly consists of mini-pillar array with electrode array for anchoring the droplets to electrochemical signal acquisition and circuit integration unit for aggregation of multiple signals. The gold nanodendrites is deposited on working electrode in 5 mg/mL $HAuCl_4$ at −0.8 V for 800 s with the optimized electrochemical performance, and the gold nanodendrites electrode has the high sensitivity and stability toward sensing multiple biomarkers. As a proof-of-concept, the mini-pillar-based individual electrochemical array have successfully detected four Alzheimer's biomarkers sensitively and simultaneously including Tau, ApoE 4, Amyloid-β and miRNA-101. This study represents the great potential to multiple and individual sensing biomarkers toward the disease early diagnosis and health monitoring.

Declaration of competing interest

The authors declare that they have no known competing financial interests or personal relationships that could have appeared to influence the work reported in this paper.

CRediT authorship contribution statement

Yongchao Song: Formal analysis, Data curation. **Tailin Xu:** Supervision. **Qinglin Zhu:** Formal analysis. **Xueji Zhang:** Funding acquisition.

Acknowledgement

We acknowledge funding from National Natural Science Foundation of China (21804007, 21890742) and National Postdoctoral Innovative Talents Support Program of China (BX20180036), China Postdoctoral Science Foundation (2019M650479).

Appendix A. Supplementary data

Supplementary data to this article can be found online at https://doi.org/10.1016/j.bios.2020.112253.

References

Atobe, M., Tateno, H., Matsumura, Y., 2018. Chem. Rev. 118 (9), 4541–4572.
Brodbelt, J.S., Morrison, L.J., Santos, I., 2019. Chem. Rev. 120 (7), 3328–3380.
Chan, H.N., Xu, D., Ho, S.L., Wong, M.S., Li, H.W., 2017. Chem. Sci. 8 (5), 4012–4018.
Chi, K.R., 2016. Nature 532 (7598), 269–271.
Chouraki, V., Seshadri, S., 2014. Adv. Genet. 87, 245–294.
Das, J., Cederquist, K.B., Zaragoza, A.A., Lee, P.E., Sargent, E.H., Kelley, S.O., 2012. Nat. Chem. 4 (8), 642–648.
Ding, S.-Y., Yi, J., Li, J.-F., Ren, B., Wu, D.-Y., Panneerselvam, R., Tian, Z.-Q., 2016. Nat. Rev. Mater. 1 (6).
Faltova, L., Kuffner, A.M., Hondele, M., Weis, K., Arosio, P., 2018. ACS Nano 12 (10), 9991–9999.
Feng, W., Ueda, E., Levkin, P.A., 2018. Adv. Mater. 30 (20), 1706111.
He, X., Xu, T., Gao, W., Xu, L.P., Pan, T., Zhang, X., 2018. Anal. Chem. 90 (24), 14105–14110.
He, X., Xu, T., Gu, Z., Gao, W., Xu, L.P., Pan, T., Zhang, X., 2019. Anal. Chem. 91 (7), 4296–4300.
Ho, S.L., Xu, D., Wong, M.S., Li, H.W., 2016. Chem. Sci. 7 (4), 2695–2700.
Hou, J., Zhang, H., Yang, Q., Li, M., Song, Y., Jiang, L., 2014. Angew. Chem. Int. Ed. 53 (23), 5791–5795.
Huebner, A., Sharma, S., Srisa-Art, M., Hollfelder, F., Edel, J.B., Demello, A.J., 2008. Lab Chip 8 (8), 1244–1254.
Hwang, H., Myong, S., 2014. Chem. Soc. Rev. 43 (4), 1221–1229.
Kalinich, M., Haber, D.A., 2018. Science 359 (6378), 866–867.
Kutter, J.P., Jacobson, S.C., Matsubara, N., Ramsey, J.M., 1998. Anal. Chem. 70 (15), 3291–3297.
Labib, M., Sargent, E.H., Kelley, S.O., 2016. Chem. Rev. 116 (16), 9001–9090.
Lee, J.K., Samanta, D., Nam, H.G., Zare, R.N., 2018. Nat. Commun. 9 (1), 1562.
Li, C., Boban, M., Snyder, S.A., Kobaku, S.P.R., Kwon, G., Mehta, G., Tuteja, A., 2016. Adv. Funct. Mater. 26 (33), 6121–6131.
Li, C., Li, X., Wei, L., Liu, M., Chen, Y., Li, G., 2015a. Chem. Sci. 6 (7), 4311–4317.
Li, J.F., Anema, J.R., Wandlowski, T., Tian, Z.Q., 2015b. Chem. Soc. Rev. 44 (23), 8399–8409.
Li, Z., Askim, J.R., Suslick, K.S., 2019. Chem. Rev. 119 (1), 231–292.
Perfezou, M., Turner, A., Merkoci, A., 2012. Chem. Soc. Rev. 41 (7), 2606–2622.
Perrin, R.J., Fagan, A.M., Holtzman, D.M., 2009. Nature 461 (7266), 916–922.
Popova, A.A., Marcato, D., Peravali, R., Wehl, I., Schepers, U., Levkin, P.A., 2018. Adv. Funct. Mater. 28 (3), 1703486.
Roy, D.S., Arons, A., Mitchell, T.I., Pignatelli, M., Ryan, T.J., Tonegawa, S., 2016. Nature 531 (7595), 508–512.
Safikhani, Z., Smirnov, P., Thu, K.L., Silvester, J., El-Hachem, N., Quevedo, R., Lupien, M., Mak, T.W., Cescon, D., Haibe-Kains, B., 2017. Nat. Commun. 8 (1), 1126.
Savelieff, M.G., Nam, G., Kang, J., Lee, H.J., Lee, M., Lim, M.H., 2018. Chem. Rev. 119 (2), 1221–1322.
Shin, S., Lee, J., Lee, S., Kim, H., Seo, J., Kim, D., Hong, J., Lee, S., Lee, T., 2017. Small 13 (7), 9.
Song, Y., Wei, W., Qu, X., 2011. Adv. Mater. 23 (37), 4215–4236.
Song, Y., Xu, T., Xu, L.P., Zhang, X., 2019. Chem. Commun. 55 (12), 1742–1745.
Su, D., Liu, X., Liu, L., Wang, L., Xie, H., Zhang, H., Meng, X., Huang, X., 2018. Adv. Funct. Mater. 28 (10), 1705699.
Xu, L.P., Chen, Y., Yang, G., Shi, W., Dai, B., Li, G., Cao, Y., Wen, Y., Zhang, X., Wang, S., 2015. Adv. Mater. 27 (43), 6878–6884.

Xu, R.H., Wei, W., Krawczyk, M., Wang, W., Luo, H., Flagg, K., Yi, S., Shi, W., Quan, Q., Li, K., Zheng, L., Zhang, H., Caughey, B.A., Zhao, Q., Hou, J., Zhang, R., Xu, Y., Cai, H., Li, G., Hou, R., Zhong, Z., Lin, D., Fu, X., Zhu, J., Duan, Y., Yu, M., Ying, B., Zhang, W., Wang, J., Zhang, E., Zhang, C., Li, O., Guo, R., Carter, H., Zhu, J.K., Hao, X., Zhang, K., 2017a. Nat. Mater. 16 (11), 1155–1161.
Xu, T., Shi, W., Huang, J., Song, Y., Zhang, F., Xu, L.P., Zhang, X., Wang, S., 2017b. ACS Nano 11 (1), 621–626.
Xu, T., Xu, L.P., Zhang, X., Wang, S., 2019. Chem. Soc. Rev. 48 (12), 3153–3165.
Ye, F., Zhao, Y., El-Sayed, R., Muhammed, M., Hassan, M., 2018a. Nano Today 18, 103–123.
Ye, L., Yang, F., Ding, Y., Yu, H., Yuan, L., Dai, Q., Sun, Y., Wu, X., Xiang, Y., Zhang, G.-J., 2018b. Adv. Funct. Mater. 1706981.
Zafari, S., Backes, C., Meese, E., Keller, A., 2015. Gerontology 61 (6), 497–503.
Zhao, Y., Bhattacharjee, S., Dua, P., Alexandrov, P.N., Lukiw, W.J., 2015. Front. Neurol. 6, 162.
Zhu, P., Kong, T., Zhou, C., Lei, L., Wang, L., 2018. Small Methods 2 (6), 1800017.